



**Quantum uncertainty effects in the dynamics of supercooled liquids: A molecular dynamics study**Gopika Krishnan  and Upendra Harbola \**Department of Inorganic and Physical Chemistry, Indian Institute of Science, Bangalore 560012, India*

(Received 23 February 2022; accepted 20 November 2022; published 13 December 2022)

Dynamics of density fluctuations in quantum supercooled liquids is analyzed using molecular dynamics simulations. In contrast to the classical case, the uncertainty in the particle position (delocalization of quantum particle in space) leads to significant differences in the dynamics of quantum liquids, both in the short- and long-time limits. The effect of uncertainty is found to be significant for length scales smaller than the uncertainty itself, and diminishes as the length scale grows. The dynamic heterogeneity of the system at short times is enhanced due to uncertainty. In the intermediate ( $\beta$ -relaxation) time regime, the heterogeneity tends to get suppressed due to quantum uncertainty. The probability distribution of particle displacements shows highly nonclassical behavior with double-peak structure at short timescales.

DOI: [10.1103/PhysRevE.106.064604](https://doi.org/10.1103/PhysRevE.106.064604)**I. INTRODUCTION**

In recent years, it has been realized that quantum effects may influence caging in supercooled liquids [1]. Indeed, quantum effects are important in understanding the anomalous temperature dependence of the specific heat ( $\propto T$ ) and the thermal conductivity ( $\propto T^2$ ) of glasses at low temperatures [2–4]. Quantum mode-coupling theory has been proposed to study the quantum effects in the dynamics of supercooled liquids [1,5–7]. Recent studies show that a crossover from fragile to strong behavior in relaxation dynamics of supercooled water can be explained by taking quantum effects into account [8–10]. The observed deviation of glass-transition temperatures in light molecular and hydrogen-bonded glass formers from the generally observed value of  $(2/3)T_m$ , where  $T_m$  is the melting temperature has been successfully explained by invoking quantum effects [8].

Tunneling and position uncertainty are two hallmarks of a quantum system. Ring-polymer molecular dynamics (RPMD), which uses the isomorphism of a quantum particle with a classical ring polymer, has been used to calculate the transport properties [11,12] and neutron scattering [13] in systems which have significant quantum effects, like parahydrogen and water. RPMD has been recently implemented to show that tunneling can lead to reentrant glassy behavior in supercooled liquids by varying the strength of quantum effects [1,7]. It has also been shown that the degree of particle delocalization leads to an additional nonclassical diffusion process and significant changes in the vibrational density of states [14]. Several works have also pointed out the effect of uncertainty in the structure of quantum liquids [1,15,16].

Here we implement RPMD to study the effects of quantum uncertainty in the dynamics of the supercooled liquid.

Using simulation and semianalytic results, we show that the so-called nonlinear effect is dependent on the quantumness of the system. The uncertainty in the position of the particle sets a length-scale cutoff beyond which such nonlinear effects are not significant. We show that the two methods give essentially the same time dependence for length scales larger than the position uncertainty quantified in terms of the radius of gyration ( $R_g$ ) [11,17] of the ring polymer, thus giving a clear physical interpretation to the dynamics observed in Kubo correlations. Quantum uncertainty leads to nonclassical features in dynamic heterogeneity in the liquid which are significant at short times.

**II. METHOD**

We employ RPMD [18,19] simulations to study the dynamics in a three-dimensional binary glass-forming quantum liquid consisting of two types of particles: A and B in the ratio 80 : 20. The interaction between two particles,  $\alpha$  and  $\beta$ , is given by the Lennard-Jones potential,  $V_{\alpha\beta}(r) = 4\epsilon_{\alpha\beta}[(\frac{\sigma_{\alpha\beta}}{r})^{12} - (\frac{\sigma_{\alpha\beta}}{r})^6]$ , where  $r$  is the distance between the two particles,  $\sigma_{\alpha\beta}$  is the effective particle size, and  $\epsilon_{\alpha\beta}$  is the interaction energy. The parameters used are  $\epsilon_{AA} = 1.0$ ,  $\epsilon_{AB} = 1.5$ ,  $\epsilon_{BB} = 0.5$ ,  $\sigma_{AA} = 1.0$ ,  $\sigma_{BB} = 0.88$ , and  $\sigma_{AB} = 0.80$ . The system consists of 1000 particles, and the density is 1.206. This mixture is known to exhibit dynamics of fragile glass-forming systems [20–22]. In the following, distance and time are in the units of  $\sigma_{AA}$  and  $\tau = \sqrt{m\sigma_{AA}^2/\epsilon_{AA}}$ , respectively, where  $m$  is the mass of a particle which is equal for both the species.

Path integral molecular dynamics (NVT) [23,24] simulation was carried out to equilibrate the system at a given temperature. From an equilibrated initial configuration, microcanonical RPMD simulation is carried out. RPMD is based on the isomorphism of a quantum particle to a classical ring polymer of  $P$  beads. This allows us to compute Kubo transformed correlation functions defined as [18,19,25]  $\tilde{c}_{AB}(t) =$

\*uharbola@iisc.ac.in

$\frac{1}{(2\pi\hbar)^{3NP}Z_P} \int d^{3NP}\mathbf{p} \int d^{3NP}\mathbf{r} e^{-\beta H_P} A_P(\mathbf{r}) B_P(\mathbf{r}, t)$ , where  $H_P = \sum_{n=1}^N \sum_{j=1}^P \frac{p_{nj}^2}{2m} + \frac{1}{2} m \omega_p^2 (\mathbf{r}_{nj} - \mathbf{r}_{n,j+1})^2 + \frac{1}{P} V(\mathbf{r}_{nj})$  is the Hamiltonian for a ring polymer containing  $P$  number of identical beads,  $\mathbf{r}_{nj}$  is the position of the  $j$ th bead in the polymer corresponding to the  $n$ th particle,  $\omega_p = 1/\beta_P \hbar$ , and  $Z_P = \frac{1}{(2\pi\hbar)^{3NP}} \int d^{3NP}\mathbf{p} \int d^{3NP}\mathbf{r} e^{-\beta H_P}$  is the partition function with  $\beta_P = \beta/P$ , where  $\beta = (k_b T)^{-1}$ . The observables  $A_P(\mathbf{r}_n)$  and  $B_P(\mathbf{r}_n)$  for the  $n$ -th particle are defined by averaging over beads of the ring polymer,  $A_P(\mathbf{r}_n) = \frac{1}{P} \sum_{i=1}^P A(\mathbf{r}_{ni})$  and  $B_P(\mathbf{r}_n) = \frac{1}{P} \sum_{i=1}^P B(\mathbf{r}_{ni})$ . In the classical case, as  $\hbar \rightarrow 0$ ,  $P \rightarrow 1$ . For the quantum case ( $\hbar \neq 0$ ), ideally  $P \rightarrow \infty$ , however, in the simulation, we fix  $P$  large enough to ensure convergence of the results with respect to  $P$  for a given quantumness  $\Lambda$  (de Broglie wavelength  $\sqrt{\frac{\hbar^2 \beta}{m}}$ ), which is manipulated by varying  $\hbar$ .

### III. RESULTS

We present the results for a fixed temperature,  $T = 1.0$ , and varying  $\Lambda^* = \Lambda/\sigma_{AA}$ . Although classically,  $T = 1.0$  corresponds to the normal liquid regime, it is possible to push the system to supercooled state by varying  $\Lambda^*$ , as shown in Ref. [1] and discussed below. Dynamics of liquids is commonly studied in terms of the relaxation of density fluctuations in the system [26–28]. A two-point density correlation function carries the essential dynamical information. The self-part of the density-correlation function is related to the dynamics of a tagged particle which shows ballistic motion in short timescales and diffusive behavior at long times [29]. The self-correlation function,  $\tilde{F}_s(k, t)$ , which characterizes relaxation of a tagged particle, is defined as (we consider an  $A$ -type particle)

$$\tilde{F}_s(k, t) = \frac{1}{N_A} \sum_{n=1}^{N_A} \langle \rho_n(k, t) \rho_n(-k, 0) \rangle, \quad (1)$$

where  $\rho_n(k, t) = \frac{1}{P} \sum_{i=1}^P e^{i\mathbf{k} \cdot \mathbf{r}_{ni}(t)}$  is the Fourier component of the  $n$ th tagged ( $A$ -type) particle density in the liquid.

Thus,  $\tilde{F}_s(k, t)$  in the quantum case can be expressed in terms of the polymer beads, which is the Kubo correlation function [13] defined as

$$\tilde{F}_s(k, t) = \frac{1}{N_A P^2} \sum_{n=1}^{N_A} \sum_{i,j=1}^P \langle e^{i\mathbf{k} \cdot [\mathbf{r}_{ni}(t) - \mathbf{r}_{nj}(0)]} \rangle, \quad (2)$$

where  $n$  is the particle index. We compare the dynamics in supercooled liquid described in terms of the Kubo correlation and the the center-of-mass (COM) correlation. We define the self-correlation function for the center of mass of the polymer as  $\tilde{F}_s^c(k, t) = \frac{1}{N_A} \sum_{n=1}^{N_A} \langle e^{i\mathbf{k} \cdot [\mathbf{R}_n(t) - \mathbf{R}_n(0)]} \rangle$ , where  $\mathbf{R}_n = \frac{1}{P} \sum_{i=1}^P \mathbf{r}_{ni}$  is the COM of the  $n$ th ring polymer. Note that the COM is a ‘‘classical’’ degree of freedom which represents the (quantum mechanical) average position of the particle. The dynamics of the Kubo correlation function obtained from RPMD may differ from the dynamics of the COM correlation function. This difference in dynamical behavior has been attributed to the nonlinearity of the density operator in Kubo correlation. However, we find that both the quantities give the

same dynamics when normalized properly, although the normalization constant depends on the length scale. For  $k \neq 0$ , the initial value  $\tilde{F}_s(k, t=0) \neq 1$ . We therefore reexpress the self-correlation function as

$$\tilde{F}_s(k, t) = \tilde{F}(k) \tilde{Q}(k, t), \quad (3)$$

where  $\tilde{F}(k) = \tilde{F}_s(k, 0)$  and  $\tilde{Q}(k, t) = \tilde{F}_s(k, t)/\tilde{F}(k)$  is the normalized correlation function.

The relaxation dynamics of the correlation functions is shown in Fig. 1(a) for different values of quantumness. Similar to the classical case [20,22], the dynamics slows down and, due to caging of the particles, the typical two-step relaxation scenario develops as  $\Lambda^*$  is increased in the moderate ( $0 < \Lambda^* \leq 0.4$ ) quantum regime, consistent with the previous observations [1,7]. This slowdown of dynamics is attributed to the increased effective size of the quantum particle, quantified by  $R_g$  [see inset of Fig. 1(a)]. Interestingly, the COM relaxation,  $\tilde{F}_s^c(k, t)$ , follows exactly the tagged particle dynamics,  $\tilde{Q}(k, t)$ , indicating that both quantities have the same dynamical information at this length scale. For larger  $k$  values, however, the two quantities show different dynamical behavior. This comparison is shown in Fig. 1(b). The  $k$  range up to which  $\tilde{Q}(k, t)$  and  $\tilde{F}_s^c(k, t)$  show the same dynamics is set by the position uncertainty in the system. It can be shown that for length scales larger than the order of position uncertainty, the relaxation of COM is captured well by  $\tilde{Q}(k, t)$ . For large length scales (small  $k$ ) where only terms up to the leading order in  $k$  are important, the COM and tagged-particle dynamics are identical (see the Appendix). However, we observe that the dynamical difference between the two quantities is only up to a  $k$ -dependent factor,  $\omega(k)$ . We show this scaling in Fig. 1(b). The solid and dashed curves show  $\tilde{Q}(k, t)$  and  $\tilde{F}_s^c(k, t)$  at  $k = 17.5$ . The brown curve denotes  $\tilde{Q}$  after scaling with  $\omega(k)$ . The scaled dynamics of  $\tilde{Q}$  is identical to  $\tilde{F}_s^c$  beyond the ballistic regime. We compare  $\tilde{F}(k)$  and  $\omega(k)$  in the inset of Fig. 1(b). At small  $k$ , both  $\tilde{F}(k)$  and  $\omega(k)$  are equal, and as  $k$  increases, they show small differences, which leads to the differences in the two scaled dynamics at short times, as shown in the main figure. These observations indicate that the long-time dynamics is mostly dictated by the large length scales ( $\gg R_g^{-1}$ ), where the position uncertainty does not play a significant role. However, the short-time dynamics is dominated by the smaller length-scale properties which are influenced by the position uncertainty. For length scales less than that of the uncertainty itself, the effect of uncertainty is evident in the tagged-particle dynamics.

In order to explore further dynamical effects of position uncertainty, we consider moments of particle displacements using COM and Kubo correlations.  $\tilde{F}_s(k, t)$  is the generator of the distribution of particle displacements in time  $t$ , and therefore contains information about all moments of the displacement. The mean square displacement (MSD) of the tagged particle is obtained as [18]

$$\begin{aligned} \langle \Delta r^2(t) \rangle &= -3 \left. \frac{d^2 \tilde{F}_s(k, t)}{dk^2} \right|_{k=0} \\ &= \frac{1}{N_A P^2} \sum_{n=1}^{N_A} \sum_{i,j=1}^P \langle [\mathbf{r}_{ni}(0) - \mathbf{r}_{nj}(t)]^2 \rangle, \quad (4) \end{aligned}$$

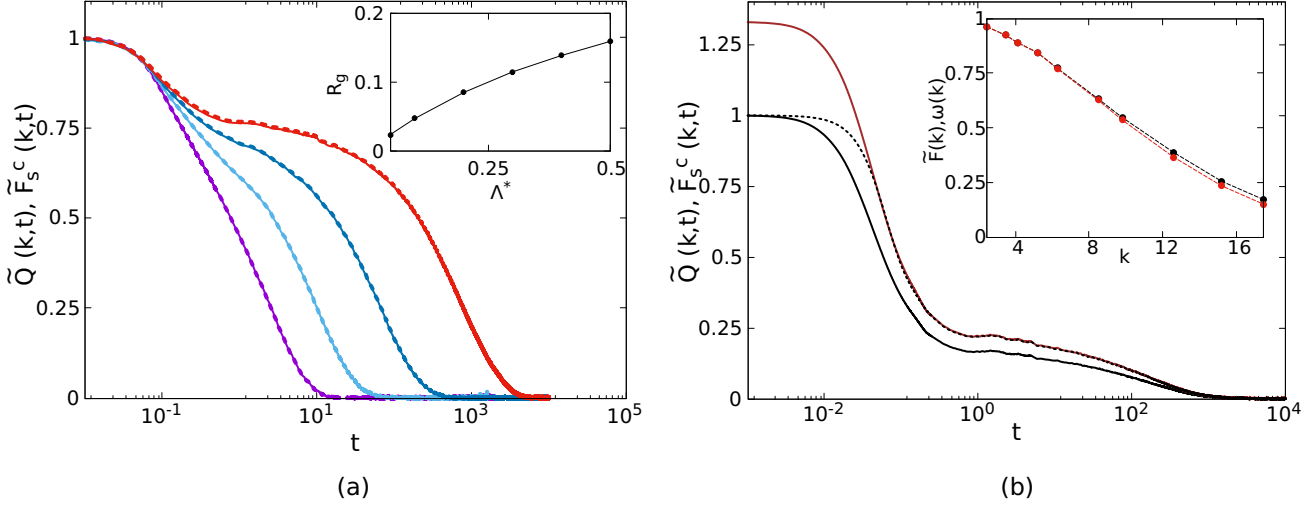


FIG. 1. (a)  $\tilde{Q}(k, t)$  (solid) and  $\tilde{F}_s^c(k, t)$  (dashed) at  $k = 7.21$  (the first peak in the structure factor) for (left to right)  $\Lambda^* = 0.05, 0.2, 0.3, 0.4$  at  $T = 1.0$ . Inset in (a) shows the  $R_g$  as a function of  $\Lambda^*$ . (b) Comparison of  $\tilde{Q}(k, t)$  and  $\tilde{F}_s^c(k, t)$  for  $k = 17.5$  (black) for  $\Lambda^* = 0.4$ . The quantity  $R_g^{-1} = 7.103$  for this  $\Lambda^*$  (see text). The brown solid line shows the scaling of  $\tilde{F}_s^c(k, t)$  to match  $\tilde{F}_s^c(k, t)$  at long times. Inset in (b) shows the comparison of the  $k$ -dependent factors  $\tilde{F}(k)$  and  $\omega(k)$  (see text for definitions).

and the next higher moment (odd moments vanish at equilibrium due to spatial homogeneity in the liquid),

$$\begin{aligned} \langle \Delta r^4(t) \rangle &= -5 \left. \frac{d^4 \tilde{F}_s(k, t)}{dk^4} \right|_{k=0} \\ &= \frac{1}{N_A P^2} \sum_{n=1}^{N_A} \sum_{j=1}^P [\mathbf{r}_{ni}(0) - \mathbf{r}_{nj}(t)]^4. \end{aligned} \quad (5)$$

Similarly,  $\tilde{F}_s^c(k, t)$  generates moments for the COM displacements.

In Fig. 2 we present a comparison of MSDs for the classical and the quantum liquids. We also show the MSD for the COM of the ring polymer ( $\langle \Delta R^2(t) \rangle$ , blue dashed lines). Interestingly, in contrast to the classical case,  $\langle \Delta r^2(0) \rangle$  has a

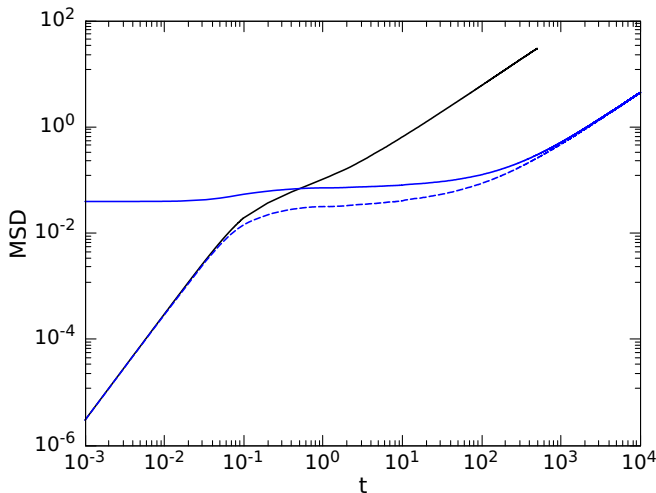


FIG. 2. Comparison of mean square displacements of the particle (blue solid line) and COM (blue dashed line) at  $T = 1.0$  for  $\Lambda^* = 0.4$ . Black solid line is the classical result.

nonzero value, and is related to the  $R_g$  of the ring polymer,  $\langle \Delta r^2(0) \rangle = 2R_g^2$ , which is the manifestation of uncertainty in the position of the quantum particle [7,16]. The MSD for the COM is the same as that of the classical particle in the ballistic regime, but changes over to the quantum MSD at the longest timescale, which is qualitatively different from the classical case, resulting in a lower diffusion coefficient. We show in the Appendix that the MSD of the COM can be expressed in terms of the tagged-particle MSD as  $\langle \Delta R^2(t) \rangle = \langle \Delta r^2(t) \rangle - 2R_g^2$ . Thus the two MSDs differ by a constant determined by the position uncertainty of the tagged particle. In the classical liquid, diffusive dynamics sets in much earlier, while the quantum liquid exhibits subdiffusive dynamics in the intermediate times due to caging resulting from increased effective size ( $\sim R_g$ ) of the quantum particle.

Using these moments, we compute dynamic heterogeneities in the relaxation dynamics of the tagged particle and the COM motion, which is quantified by the non-Gaussian (heterogeneity) parameter,  $\alpha_2(t)$ , defined as [30]  $\alpha_2(t) = \frac{3\langle \Delta r^4(t) \rangle}{5\langle \Delta r^2(t) \rangle^2} - 1$ .  $\alpha_2(t) = 0$  when the distribution is a Gaussian, and is nonzero otherwise. Dynamic heterogeneity has been well studied in simple models as well as real systems, like water, using simulation methods [31–33]. It typically grows from zero as time evolves, reaches a maximum in the intermediate timescale of caging, and decays to zero at long, diffusive timescales. This is depicted in Fig. 3. The heterogeneities are clearly very different for the tagged particle and the COM dynamics. The COM shows a classical-like dynamic heterogeneity with a peak in the intermediate ( $\beta$ -relaxation) timescale and decays to zero at the longest times where the dynamics becomes diffusive. On the other hand, the tagged-particle dynamics exhibits qualitative differences: it starts from a nonzero value and decays to a small value in the ballistic time regime, before it starts to increase again. Similar nonzero  $\langle \Delta r^2(0) \rangle$  and qualitative behavior of the Kubo-transformed tagged-particle dynamics has been observed in

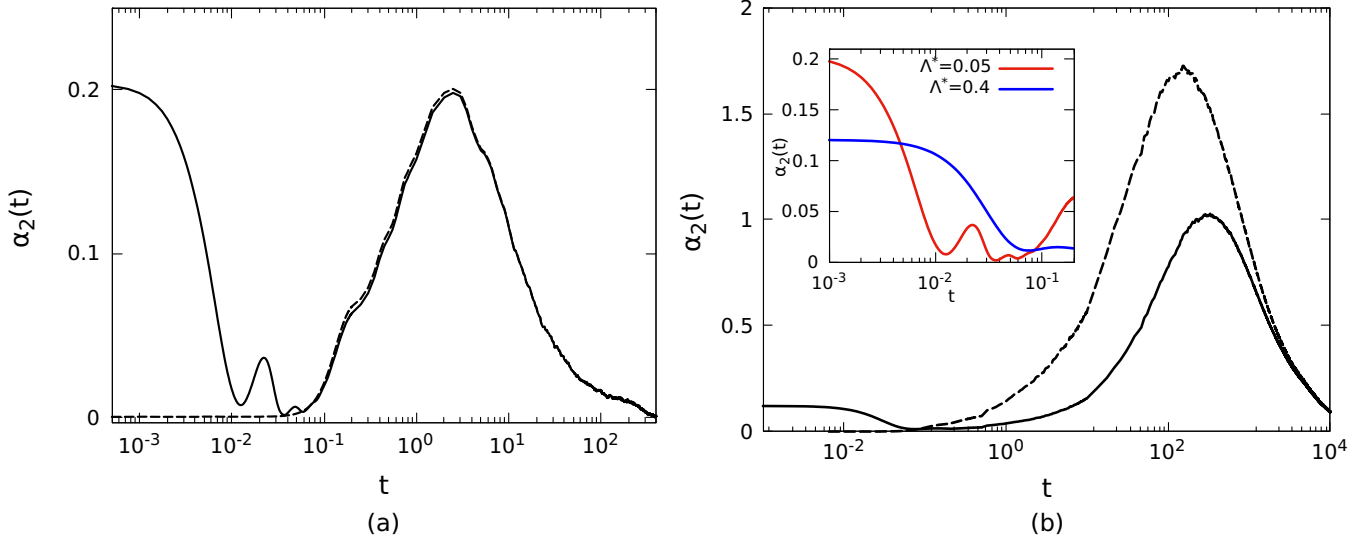


FIG. 3. Non-Gaussian parameter [ $\alpha_2(t)$ ] of tagged particle (solid lines) and COM (dashed lines) for two different values of quantumness (a)  $\Lambda^* = 0.05$ , (b)  $\Lambda^* = 0.4$  at  $T = 1.0$ . Inset in (b) shows a comparison of  $\alpha_2(t)$  in the ballistic regime for the two cases.

hard-sphere systems using quantum mode-coupling formulation [34].

Beyond the ballistic regime, for smaller  $\Lambda^*$ , heterogeneities in the COM and the tagged-particle dynamics are almost identical [Fig. 3(a)]. At higher  $\Lambda^*$  [Fig. 3(b)], heterogeneity in the COM and the particle motion shows expected behavior at longer times: its amplitude grows and the peaks shift to higher times, indicating that the caging is more robust and remains for longer times. More interestingly, however, the tagged-particle and the COM dynamics now exhibit very different behavior even at longer times. The COM motion is more heterogeneous and attains the maximum earlier than the heterogeneity in the tagged-particle dynamics. Thus for higher quantumness, the tagged particle shows more heterogeneous dynamics over shorter times [see inset of Fig. 3(b)] as compared to the COM, while the COM motion is more heterogeneous over the longer times. As we discuss in the Appendix, this behavior can be attributed to the quantum effects arising due to the initial uncertainty in the tagged-particle position. The distribution of tagged-particle displacements in time  $t$ ,  $G_s(r, t)$ , can be obtained by taking Fourier transform of Eq. (3). This gives  $G_s(r, t) = \int dr' G_s(r') G(|r - r'|, t)$ , where  $G(r, t)$  is the Fourier transform of  $\tilde{Q}(k, t)$ . This shows how the tagged-particle dynamics at time  $t$  is correlated to its initial distribution (position uncertainty), while for the COM dynamics no such correlation exists as the initial distribution  $G_s(r) = \delta(r)$ , just like the classical case. As discussed in the Appendix, as a result of this dependence on the initial distribution, the tagged-particle heterogeneity is suppressed below the (classical-like) COM heterogeneity at longer times, while it is enhanced at shorter, ballistic times.

The distribution functions for the COM and the tagged-particle displacements are depicted in Fig. 4. At short times, the distribution function shows double-peak structure: a sharp peak at small  $r$  [top inset in Fig. 4(a)] and a broader peak at larger  $r$ . This indicates that quantum nature tends to delocalize the particle, and its position over smaller times cannot

be assigned to the displacement of COM which exhibits a Gaussian-like distribution (dashed curve), well described by  $\sim \sqrt{\frac{3}{2\pi \langle r^2(t) \rangle}} e^{-3r^2/2 \langle r^2(t) \rangle}$  (not shown) in the ballistic regime. As time increases, the weight of the first peak in the particle distribution decreases and it becomes similar to the COM distribution [lower inset in Fig. 4(a)] in the timescale beyond the ballistic regime. However, at larger quantumness [Fig. 4(b)], although the first peak in particle distribution diminishes, the distribution remains distinct from the COM distribution even at longer times.

#### IV. CONCLUSIONS

The results presented here clearly demonstrate the effects of quantum uncertainty in the dynamics of supercooled liquids. The relaxation dynamics of the COM and the tagged-particle density correlation functions show similar behavior over length scales larger than the position uncertainty of quantum particles in the system ( $\sim R_g$ ). However, at shorter length scales, the two quantities differ significantly. This results in their dynamical heterogeneities being different. The COM motion shows classical-like dynamic heterogeneity, while the heterogeneity associated with the tagged-particle dynamics exhibits nonclassical features. The nonclassical behavior at smaller times is enhanced due to stronger dynamical correlations between quantum uncertainty in the particle positions at the initial time and that at time  $t$ . These quantum effects lead to highly non-Gaussian and nonclassical features in the distribution of the tagged-particle displacements. At short times, the COM position is distributed classically according to a Gaussian distribution, but the tagged-particle position follows a double-peak distribution which becomes classical-like at longer timescales. The short-time features discussed here are not specific to the supercooled state, but is expected in any system with significant quantum effects. Quantum uncertainty also affects the magnitude of the tagged-particle dynamic heterogeneity at the  $\beta$ -relaxation timescales, and tends to suppress it. Thus, the quantum uncertainty not only



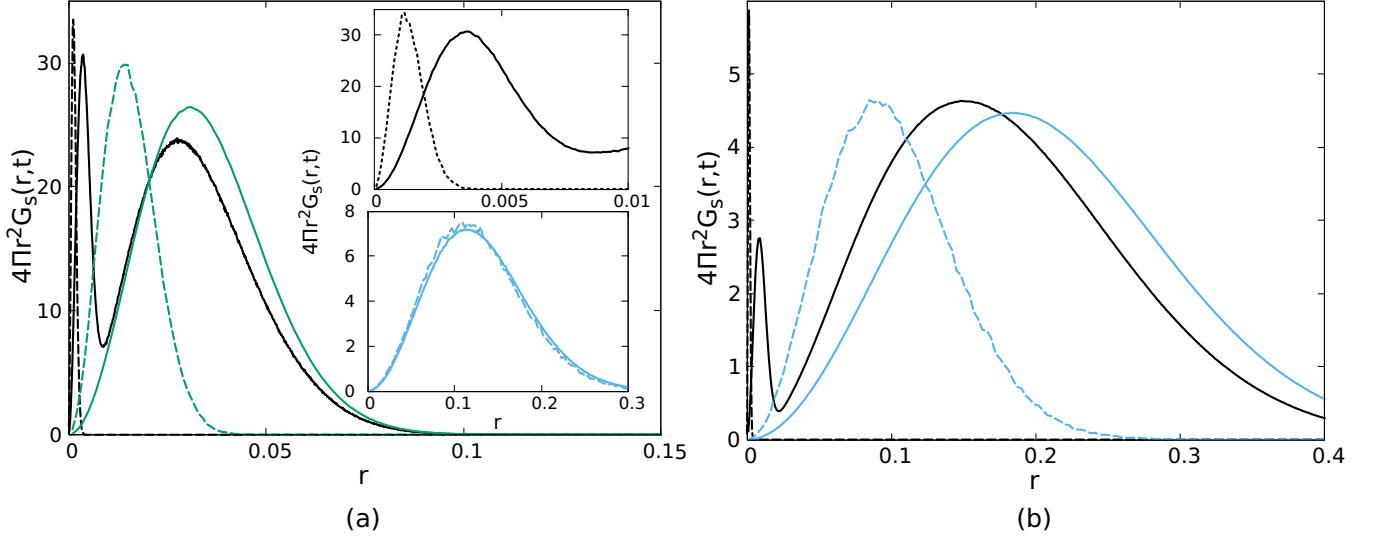


FIG. 4. (a) Probability distribution of displacements [ $G_s(r, t)$ , solid lines] for  $\Lambda^* = 0.05$  for times  $t = 10^{-3}$  (black),  $10^{-2}$  (green), and  $10^{-1}$  (blue, bottom inset). The top inset shows the first peak for  $t = 10^{-3}$ . (b) Same as (a) but for higher quantumness,  $\Lambda^* = 0.4$  at  $T = 1.0$ . Dashed curves represent the results for the COM and, for visual clarity, have been divided by 20 (black) and 2 (green) for  $\Lambda^* = 0.05$ , and 100 (black) and 2 (blue) for  $\Lambda^* = 0.4$ .

affects the short-time, but also the long-time dynamics of the system.

Although the beads in a ring polymer do not have a physical meaning, nevertheless, the two-peak structure in particle distribution can be assigned to the correlations among the beads in the tagged-particle ring polymer. The sharper peak at smaller times is due to the self-correlation of beads while the broader peak at longer times is caused by the cross correlation among the beads, representing the quantum uncertainty in the particle position.

#### ACKNOWLEDGMENTS

G.K. acknowledges the support from Council of Scientific and Industrial Research, India. U.H. acknowledges Scientific and Engineering Research Board of India for support under Grant No. CRG/2020/001110.

#### APPENDIX

##### 1. Comparison of the tagged-particle and COM dynamics

We can define the COM self-correlation, as in the main text,  $\tilde{F}_s^c(k, t) = \frac{1}{N_A} \sum_{n=1}^{N_A} \langle e^{ik \cdot [\mathbf{R}_n(t) - \mathbf{R}_n(0)]} \rangle$ , where  $\mathbf{R}_n = \frac{1}{P} \sum_{i=1}^P \mathbf{r}_{ni}$  is the COM of the  $n$ th ring polymer. The center-of-mass MSD is defined as

$$\begin{aligned} \langle \Delta R^2(t) \rangle &= \frac{1}{N_A} \sum_{n=1}^{N_A} \langle [\mathbf{R}_n(0) - \mathbf{R}_n(t)]^2 \rangle \\ &= \frac{1}{N_A P^2} \sum_{n=1}^{N_A} \sum_{i,j=1}^P \langle [\mathbf{r}_{ni}(0) - \mathbf{r}_{ni}(t)][\mathbf{r}_{nj}(0) - \mathbf{r}_{nj}(t)] \rangle. \end{aligned} \quad (\text{A1})$$

This gives

$$\langle \Delta R^2(t) \rangle = \langle \Delta r^2(t) \rangle - 2R_g^2, \quad (\text{A2})$$

where  $\langle \Delta r^2(t) \rangle$  is the tagged-particle MSD, as defined in Eq. (4). Thus the MSD of the COM and the tagged particle are trivially related though the uncertainty in the particle position.

The normalized Kubo-transformed tagged-particle dynamics,  $\tilde{Q}(k, t) = \tilde{F}_s(k, t)/\tilde{F}(k)$ . Using small  $k$  expansion, and retaining terms up to  $k^2$  order, we have

$$\begin{aligned} \tilde{Q}(k, t) &= 1 - \frac{k^2}{3!} (\langle \Delta r^2(t) \rangle - 2R_g^2) \\ &= 1 - \frac{k^2}{3!} \langle \Delta R^2(t) \rangle \\ &\approx \tilde{F}_s^c(k, t). \end{aligned} \quad (\text{A3})$$

Thus, from Eqs. (2) and (A2), we see that for small  $k$ ,  $\tilde{Q}(k, t) = \tilde{F}_s^c(k, t)$ . For higher  $k$  ( $\gg 1/R_g$ ) values, the two quantities show differences. This can be understood observing the fact that for  $k > 1/R_g$  the dynamics is being probed at the microscopic length scales, where the spread of the ring polymer affects the dynamics. The COM, on the other hand, being a single degree of freedom, is not affected by this.

##### 2. Comparison of $\alpha_2(t)$ of the tagged particle and COM

Moments of the tagged-particle displacement at time  $t$  can be obtained by taking derivatives of the function  $\tilde{F}_s(k, t)$  defined in Eq. (3) in the main text. The first two moments given in Eqs. (4) and (5) in the main text can be rewritten as

$$\langle \Delta r^2(t) \rangle = -3 \tilde{F}_s^{(2)}(k, t)|_{k=0} = -3(\tilde{Q}^{(2)} + \tilde{F}^{(2)}), \quad (\text{A4})$$

$$\langle \Delta r^4(t) \rangle = 5 \tilde{F}_s^{(4)}(k, t)|_{k=0} = 5(\tilde{F}^{(4)} + 6\tilde{F}^{(2)}\tilde{Q}^{(2)} + \tilde{Q}^{(4)}), \quad (\text{A5})$$

where the  $n$ th derivative with respect to  $k$  at  $k = 0$  is denoted by superscript “ $(n)$ ” and we have used  $\tilde{F}(0) = 1$ , and  $\tilde{F}^{(1)}(0) = \tilde{F}^{(3)}(0) = 0$ , because of the spatial homogeneity in the system, and the dependence on time of the function  $\tilde{Q}^{(n)}(t)$

is suppressed for brevity. Using this,  $\alpha_2(t)$  can be written as

$$\alpha_2(t) = \frac{1}{3} \frac{\tilde{Q}^{(4)}}{(\tilde{Q}^{(2)})^2} \left[ 1 + 6 \frac{\tilde{F}^{(2)}}{\tilde{Q}^{(2)}} + \frac{\tilde{F}^{(4)}}{\tilde{Q}^{(2)}} \right] - 1. \quad (\text{A6})$$

Note that  $\tilde{Q}^{(2)} = -(1/3)\langle \Delta R^2(t) \rangle$  [see Eq. (A3)], which decreases monotonously with time, while  $\tilde{F}^{(2)} = -(2/3)R_g^2$ . In the timescale of  $\beta$  relaxation,  $|\tilde{Q}^{(2)}| \gg |\tilde{F}^{(2)}|$ , hence the ratio  $\frac{\tilde{F}^{(2)}}{\tilde{Q}^{(2)}} \ll 1$ , and  $\alpha_2(t)$  can be approximated as

$$\begin{aligned} \alpha_2(t) &= \alpha_2^c(t) - c(t), \\ c(t) &= \frac{1}{3} \left( \frac{\tilde{F}^{(2)}}{\tilde{Q}^{(2)}} \right)^2 \left[ 12 + 2 \frac{\tilde{F}^{(4)}}{\tilde{F}^{(2)}\tilde{Q}^{(2)}} + 6 \frac{\tilde{F}^{(2)}}{\tilde{Q}^{(2)}} + \frac{\tilde{F}^{(4)}}{(\tilde{Q}^{(2)})^2} \right] \\ &= \frac{4}{27} \left( \frac{R_g^2}{\tilde{Q}^{(2)}} \right)^2 \left[ 12 - 3 \frac{\tilde{F}^{(4)}}{R_g^2\tilde{Q}^{(2)}} - 4 \frac{R_g^2}{\tilde{Q}^{(2)}} + \frac{\tilde{F}^{(4)}}{(\tilde{Q}^{(2)})^2} \right]. \end{aligned} \quad (\text{A7})$$

Here  $\alpha_2^c(t) = \frac{1}{3} \frac{\tilde{Q}^{(4)}}{(\tilde{Q}^{(2)})^2} - 1$  is the dynamic heterogeneity of a classical-like system. If  $R_g = 0$ , which is the case for a classical system, this gives  $c(t) = 0$  and  $\alpha_2(t) = \alpha_2^c(t)$ . Thus, the term  $c(t)$  represents the effects of uncertainty on the dynamical heterogeneity. Since  $\tilde{Q}^{(2)} \leq 0$ ,  $\tilde{F}^{(2)} \leq 0$  and  $\tilde{Q}^{(4)} \geq 0$ ,  $c(t) \geq 0$ , this implies that the quantum uncertainty tends to suppress dynamical heterogeneity in ( $\beta$ -relaxation) longer times, as discussed in the main text.

In the short (ballistic) timescale, the position of the  $i$ th bead of particle  $n$  at time  $t$  can be approximated as  $\mathbf{r}_{ni}(t) \approx \mathbf{r}_{ni}(0) + t\mathbf{v}_{ni}(0)$ , where  $\mathbf{v}_{ni}(0)$  is the initial velocity of the particle. Substituting this in Eq. (2) of the main text, we can write

$$\begin{aligned} \tilde{F}_s(k, t) &= \frac{1}{N_A P^2} \sum_{n=1}^{N_A} \sum_{i,j=1}^P \langle \exp(i\mathbf{k} \cdot [\mathbf{r}_{ni}(0) - \mathbf{r}_{nj}(0)]) \rangle \\ &\quad \times \exp(i\mathbf{k} \cdot \mathbf{v}_{ni}(0)t). \end{aligned} \quad (\text{A8})$$

Here it is to be noted that once we have mapped the quantum particle onto a ring polymer, the polymer beads are to be treated classically and  $\mathbf{r}_{ni}$  commutes with  $\mathbf{v}_{ni}$  at the same time, as they are not operators anymore. As the initial positions and velocities of beads are uncorrelated, we can write

$$\begin{aligned} \tilde{F}_s(k, t) &= \frac{1}{N_A P^2} \sum_{n=1}^{N_A} \sum_{i,j=1}^P \langle \exp(i\mathbf{k} \cdot [\mathbf{r}_{ni}(0) - \mathbf{r}_{nj}(0)]) \rangle \\ &\quad \times \langle \exp(i\mathbf{k} \cdot \mathbf{v}_{ni}(0)t) \rangle. \end{aligned} \quad (\text{A9})$$

Since the system is isotropic,  $\mathbf{v}_{ni}(0)$  is distributed according to the Boltzmann distribution such that  $\langle \mathbf{v}_{ni}^2 \rangle = \langle \mathbf{v}^2 \rangle$  for all  $n$  and  $i$ , determined by the temperature alone. This allows us to write

$$\begin{aligned} \tilde{F}_s(k, t) &= \frac{1}{N_A P^2} \sum_{n=1}^{N_A} \sum_{i,j=1}^P \langle \exp(i\mathbf{k} \cdot [\mathbf{r}_{ni}(0) - \mathbf{r}_{nj}(0)]) \rangle \\ &\quad \times \exp\left(-\frac{k^2}{6} \langle \mathbf{v}^2 \rangle t^2\right) \\ &= \tilde{F}(k)\tilde{Q}(k, t), \end{aligned} \quad (\text{A10})$$

where we identify  $\tilde{Q}(k, t) = \exp(-\frac{k^2}{6} \langle \mathbf{v}^2 \rangle t^2)$ . Using the above relation in Eq. (A6), we obtain

$$\alpha_2(t) = \frac{3\langle \Delta r^4(0) \rangle - 5\langle \Delta r^2(0) \rangle^2}{45\langle \mathbf{v}^2 \rangle^2 t^4 + 30\langle \mathbf{v}^2 \rangle t^2 \langle \Delta r^2(0) \rangle + 5\langle \Delta r^2(0) \rangle^2}. \quad (\text{A11})$$

In the classical case (also true for the COM motion),  $\langle \Delta r^2(0) \rangle = \langle \Delta r^4(0) \rangle = 0$  and  $\alpha_2(t) = 0$  in the ballistic regime. However, for a quantum particle  $|\alpha_2(t)| \neq 0$ , as reported in the main text. Although, from the above Eq. (A11),  $\alpha_2(t)$  can be positive or negative, in our simulation we find that quantum effects always give  $\alpha_2(t) > 0$  in the short timescale, that is,  $\frac{\langle \Delta r^4(0) \rangle}{(\langle \Delta r^2(0) \rangle)^2} > \frac{5}{3}$ .

- 
- [1] T. E. Markland, J. A. Morrone, B. J. Berne, K. Miyazaki, E. Rabani, and D. R. Reichman, *Nat. Phys.* **7**, 134 (2011).  
[2] R. Zeller and R. Pohl, *Phys. Rev. B* **4**, 2029 (1971).  
[3] P. W. Anderson, B. I. Halperin, and C. M. Varma, *Philos. Mag.* **25**, 1 (1972).  
[4] D. Khomenko, C. Scalliet, L. Berthier, D. R. Reichman, and F. Zamponi, *Phys. Rev. Lett.* **124**, 225901 (2020).  
[5] D. R. Reichman and E. Rabani, *Phys. Rev. Lett.* **87**, 265702 (2001).  
[6] E. Rabani and D. R. Reichman, *Annu. Rev. Phys. Chem.* **56**, 157 (2005).  
[7] T. E. Markland, J. A. Morrone, K. Miyazaki, B. J. Berne, D. R. Reichman, and E. Rabani, *J. Chem. Phys.* **136**, 074511 (2012).  
[8] V. N. Novikov and A. P. Sokolov, *Phys. Rev. Lett.* **110**, 065701 (2013).  
[9] C. Gainaru, A. L. Agapov, V. Fuentes-Landete, K. Amann-Winkel, H. Nelson, K. W. Köster, A. I. Kolesnikov, V. N. Novikov, R. Richert, R. Böhmer, T. Loerting, and A. P. Sokolov, *Proc. Natl. Acad. Sci. USA* **111**, 17402 (2014).  
[10] V. Novikov and A. Sokolov, *Eur. Phys. J. E* **40**, 57 (2017).  
[11] T. F. Miller and D. E. Manolopoulos, *J. Chem. Phys.* **122**, 184503 (2005).  
[12] T. F. Miller and D. E. Manolopoulos, *J. Chem. Phys.* **123**, 154504 (2005).  
[13] I. R. Craig and D. E. Manolopoulos, *Chem. Phys.* **322**, 236 (2006).  
[14] J. Lan, V. Kapil, P. Gasparotto, M. Ceriotti, M. Iannuzzi, and V. V. Rybkin, *Nat. Commun.* **12**, 766 (2021).  
[15] L. M. Sesé and R. Ledesma, *J. Chem. Phys.* **106**, 1134 (1997).  
[16] S. Miura, S. Okazaki, and K. Kinugawa, *J. Chem. Phys.* **110**, 4523 (1999).  
[17] T. F. Miller, *J. Chem. Phys.* **129**, 194502 (2008).  
[18] I. R. Craig and D. E. Manolopoulos, *J. Chem. Phys.* **121**, 3368 (2004).  
[19] M. E. Tuckerman, *Statistical Mechanics: Theory and Molecular Simulations* (Oxford University Press, New York, 2010).  
[20] W. Kob and H. C. Andersen, *Phys. Rev. Lett.* **73**, 1376 (1994).  
[21] W. Kob and H. C. Andersen, *Phys. Rev. E* **51**, 4626 (1995).

- [22] W. Kob and H. C. Andersen, *Phys. Rev. E* **52**, 4134 (1995).
- [23] S. Plimpton, *J. Comput. Phys.* **117**, 1 (1995).
- [24] R. Freitas, M. Asta, and V. V. Bulatov, *npj Comput. Mater.* **4**, 55 (2018).
- [25] S. Habershon, D. E. Manolopoulos, T. E. Markland, and T. F. Miller III, *Annu. Rev. Phys. Chem.* **64**, 387 (2013).
- [26] A. Rahman, K. S. Singwi, and A. Sjölander, *Phys. Rev.* **126**, 986 (1962).
- [27] J.-P. Hansen and I. R. McDonald, *Theory of Simple Liquids*, 3rd ed. (Academic, Burlington, 2006), pp. 178–218.
- [28] S. P. Das, *Statistical Physics of Liquids at Freezing and Beyond* (Cambridge University Press, Cambridge, UK, 2011).
- [29] L. Larini, A. Ottochian, C. De Michele, and D. Leporini, *Nat. Phys.* **4**, 42 (2008).
- [30] A. Rahman, *Phys. Rev.* **136**, A405 (1964).
- [31] W. Kob, C. Donati, S. J. Plimpton, P. H. Poole, and S. C. Glotzer, *Phys. Rev. Lett.* **79**, 2827 (1997).
- [32] F. Sciortino, P. Gallo, P. Tartaglia, and S. H. Chen, *Phys. Rev. E* **54**, 6331 (1996).
- [33] N. Giovambattista, M. G. Mazza, S. V. Buldyrev, F. W. Starr, and H. E. Stanley, *J. Phys. Chem. B* **108**, 6655 (2004).
- [34] A. Das, G. Krishnan, E. Rabani, and U. Harbola, *Phys. Rev. E* **105**, 054136 (2022).